

# On the low frequency component of the ENSO-Indian Monsoon relationship; a paired proxy perspective

M. Berkelhammer<sup>1,2</sup>, A. Sinha<sup>3</sup>, M. Mudelsee<sup>4,5</sup>, H. Cheng<sup>6,7</sup>, K. Yoshimura<sup>8,9</sup>, and J. Biswas<sup>10</sup>

<sup>1</sup>University of Colorado, Boulder

<sup>2</sup>Cooperative Institute for Research in Environmental Sciences

<sup>3</sup>California State University, Dominguez Hills

<sup>4</sup>Climate Risk Analysis

<sup>5</sup>Alfred Wegener Institute, Bremerhaven

<sup>6</sup>University of Minnesota, Minneapolis

<sup>7</sup>Institute for Global Environmental Change, Xian Jiatong

<sup>8</sup>Atmospheric and Oceanic Research Institute, Tokyo

<sup>9</sup>Scripps Institute for Oceanography, La Jolla

<sup>10</sup>National Cave Research and Protection Organization, Raipur

*Correspondence to:* Max Berkelhammer  
(max.berkelhammer@colorado.edu)

**Abstract.** There are a number of clear examples in the instrumental period where positive ENSO events were coincident with a severely weakened summer monsoon over India (ISM). ENSO's influence on the Indian Monsoon has therefore remained the centerpiece of various predictive schemes of ISM rainfall for over a century. The teleconnection between the monsoon and ENSO has undergone a protracted weakening since the late 1980's suggesting the strength of ENSO's influence on the monsoon may vary considerably on multidecadal timescales. The recent weakening has occurred despite the fact that the ENSO system has experienced variance levels during the latter part of the 20<sup>th</sup> century that are as high as any period in the past millennium. The recent change in the ENSO-ISM coupling has prompted questions as to whether this shift represents a natural mode of climate variability or a fundamental change in ENSO and/or ISM dynamics due to anthropogenic warming or aerosol impacts on the monsoon. The brevity of empirical observations and large systematic errors in the representation of these two systems in state-of-the-art general circulation models hamper efforts to reliably assess the role ENSO plays in generating low frequency variance in the ISM. Here we place the 20<sup>th</sup> century ENSO-ISM relationship in a millennial context by assessing the phase relationship between the two systems across the time spectrum using a series of high resolution reconstructions of ENSO and the ISM from tree rings, speleothems and

corals. The results from all the proxies suggest that in the high-frequency domain (5-15 years), warm (cool) sea surface temperature in the eastern Tropical Pacific lead to a weakened (strengthened) monsoon. This finding is consistent with the observed relationship between the two systems during the instrumental period. However, in the multidecadal domain (30-90 years) the phasing between the systems is reversed such that periods of strong monsoons were, in general, coincident with periods of enhanced ENSO variability. This result is counterintuitive to the expectation that enhanced ENSO variance favors an asymmetric increase in the frequency of El Niño events and therefore a weakened monsoon system. The results suggest that the prominent multidecadal variability that characterizes the last 1,000 years of the ISM is not likely attributable to shifts in ENSO variability. If there is a continued trend towards enhanced ENSO variance in the coming decades, the results presented here do not suggest this will force a weakening of the Indian Monsoon system.

---

## 1 Introduction

An improved understanding of the dynamical relationship between the El Niño/Southern Oscillation (ENSO) and the Indian Summer Monsoon (ISM), has significant value in constraining future projections of the monsoon system. The

50 ENSO-related Indo-Pacific tropical sea surface temperature (SST) anomalies have been considered as the dominant externally-driven forcing of monsoon variability (Webster et al., 1998; Kumar et al., 2006). The dynamical linkage between these two systems principally results from the  
 55 SST-induced east-west shifts in the Walker circulation and its interaction with the regional monsoon Hadley circulation (Webster et al., 1998; Krishnamurthy and Goswami, 2000; Ashok et al., 2004). For example, El Niño's impact on ISM rainfall is particularly strong when the locus of deep atmospheric convection shifts to the central Pacific (Central El Niño) and the strongest descending lobe of the Walker cell is focused over the eastern equatorial Indian Ocean (Fasullo and Webster, 2002; Kumar et al., 1999, 2006) - driving an anomalous monsoon Hadley circulation whose descending limb suppresses the convection-driven monsoon rainfall over the Indian sub-continent. The extreme manifestation of this coupling is exemplified (albeit, sporadically) by the co-occurrence of large El Niño events and devastating droughts in the Indian sub-continent such as during 1876-78, 1918-19, and 1982-83 (Kumar et al., 2006).

In observational data, the strength of the ENSO-ISM relationship (characterized by linear correlations between any of the broad indices of ISM rainfall and SST anomalies in the tropical Pacific, respectively) has varied on inter-decadal to multidecadal timescales exhibiting high (low) inverse-correlations at times when the ENSO variance shows high (low) amplitude modulation (Torrence and Webster, 1999; Krishnamurthy and Goswami, 2000). This has led to the suggestion that ENSO influences ISM rainfall through the same physical mechanism on both interannual and interdecadal timescales and that the waxing and waning of the coupling is related to frequency/amplitude modulation of ENSO events and changes in the tropical Pacific mean state (Torrence and Webster, 1999). The recent breakdown in the relationship between the two systems (e.g. Kumar et al. (1999)) has however, occurred in the context of increased ENSO variance since the 1980's, with the late 20<sup>th</sup> century ENSO variability reaching a level as high as any other period during the last millennium (Li et al., 2011; Cobb et al., 2003, 2013). A range of hypotheses have been offered to explain the recent breakdown including global warming (Kumar et al., 1999), a southeastward shift of the subsiding limb of the Walker cell (Collins et al., 2010), changes in ENSO spatial characteristics (Kumar et al., 2006), and the co-occurrence of ENSO and Indian Ocean Dipole (IOD) events (Ashok et al., 2004; Ummenhofer et al., 2011). In contrast, it has been argued that the relationship has largely remained intact and any fluctuations in its strength are merely a sampling artifact such that low frequency changes in the correlation statistics between ENSO and the ISM timeseries' occurs much in the manner expected from purely stochastic processes (Gershunov et al., 2001).

Understanding the nature of the ENSO-ISM relationship and specifically constraining the dynamics that have generated the recent change in the coupling between the systems is a problem ideally suited for state-of-the-art general circulation models (e.g. Jourdain et al. (2013)) where the response of the systems to various forcing mechanisms could be tested. However, systematic errors in simulating the mean state and variability of both ENSO and the ISM systems has hampered the ability to utilize this tool (Annamalai et al., 2007; Collins et al., 2010). Therefore, neither empirical observations, because of their brevity, nor model simulations are adequate in assessing the long-term nature of the influence that ENSO has on the ISM. As a consequence, there are significant limits on the predictability of the monsoon system across timescales. For example, if the recent increase in ENSO variance represents a long term trends towards a more active ENSO system, than it would be important to predict whether this would lead to a shift in the mean state of the monsoon. Proxy reconstructions of ENSO and ISM can therefore provide much needed constraints on the nature of this coupling, particularly in the low frequency domain under varying climate boundary conditions. Here we utilize a number of recent high-resolution, well-dated reconstructions of the two systems from tree rings, speleothems and corals to test whether multi-decadal shifts in ENSO variance have a consistent influence on the ISM system.

## 2 Methods

### 2.1 Monsoon Reconstructions

A number of previous studies (e.g. Berkelhammer et al. (2010); Sinha et al. (2007, 2011)) have demonstrated that ISM variability can be robustly reconstructed on a variety of timescales using the isotopic variability ( $\delta^{18}\text{O}$ ) of speleothems from central India. Here we utilize a continuous 1400-year long ISM reconstruction derived from a pair of overlapping speleothems from two sites, Dandak and Jhumar Caves, located at  $\sim 19^\circ\text{N}$ ;  $82^\circ\text{E}$  in the southern region of the core monsoon zone (CMZ) defined here as  $\sim 18^\circ\text{-}27^\circ\text{N}$  and  $69^\circ\text{-}88^\circ\text{E}$  (Fig. 1). Details on the sampling methodologies and age models of these two records are described in previous studies (Berkelhammer et al., 2010; Sinha et al., 2011) and for the purpose of this study we have taken the two published records (available here: <http://www.ncdc.noaa.gov/paleo/speleothem.html>), linearly interpolated them to an annual timescale and averaged the two (over the period of overlap) to produce a composite  $\delta^{18}\text{O}$  record. We deem this compositing valid as the  $\delta^{18}\text{O}$  profiles from Jhumar (AD 2007-1075) and Dandak (AD 1562-625) are well correlated (over the period of overlap) at  $r = 0.62$  ( $n = 353$ ; 95% [0.43; 0.74]) suggesting the independent age models are robust and the isotopic variability

ity is not a function of the local cave environment (Figure 1)t.

There is a significant (inverse) correlation between the speleothem  $\delta^{18}\text{O}$  and CMZ JJAS precipitation (defined as the average of instrumental JJAS precipitation from  $18^\circ$  to  $27^\circ\text{N}$  and  $69^\circ$  to  $88^\circ\text{E}$ ) timeseries' during the instrumental period (AD 1903–2006,  $n = 70$ ,  $r = -0.46$  with 95% CI [-0.59; -0.32]) (Fig. 1). Significance and confidence intervals for the correlation estimates were obtained using block bootstrap resampling (Mudelsee, 2010), which takes into account deviations from normal distributional shape and temporal autocorrelation. Further validation of the skill of this proxy comes from the observation that the record captures a number of known historical droughts such as those during AD 1876–78, 1861–63, and 1790–96 (Sinha et al., 2007) and captures the series of protracted regional monsoon “megadroughts” in the late 14<sup>th</sup> century observed in tree ring records from SE Asia (Buckley et al., 2010).

The robustness of the speleothems in capturing monsoon variability arises from the presence of a strong “amount effect” (Dansgaard, 1964) over south Asia, which has been documented in both modeling and observational studies (Dayem et al., 2010; Vuille et al., 2005; Pausata et al., 2011). In order to test the regional manifestation of the “amount effect” (i.e. its persistence and strength), we utilize simulations with a nudged Isotope-enabled GCM, IsoGSM, (Yoshimura et al., 2008), which has been validated for parts of India in a previous study (Berkelhammer et al., 2012). The model shows that the region from where this proxy was generated experiences a strong inverse relationship between the  $\delta^{18}\text{O}$  in the precipitation ( $\delta^{18}\text{O}_p$ ) and the modeled area-weighted precipitation amount over the CMZ (Fig. 2). Similar (or even more significant) correlation coefficients are also found for other broad ISM rainfall indices in the isotope simulations such as the Homogenous Monsoon Zone and the Indian Monsoon Index (IMI) (Wang and Fan, 1999; Wang et al., 2009), indicating the isotopic ratio in the precipitation at this site is a broad indicator of monsoon strength and not sensitive to domain boundaries or the choice of index.

The sensitivity of the isotopes in the precipitation, and consequently the proxy, to the overall strength of the Indian Monsoon system arises because of its location at the near distal end of the landward portion of the low level Jet that is the primary conduit for moisture transport from the Arabian Sea onto the Indian subcontinent (Fig. 2). As a consequence, the isotopic ratio in the vapor and the precipitation at this site aggregate all upstream processes (e.g. rain-out) that have influenced the Arabian Sea branch of the monsoon system as it crosses the continent (Fig. 2). For example, mean westerly flow is weaker with a large reduction in moisture flux during anomalous monsoon seasons associated with El Niño events (Fasullo and Webster, 2002). The low level jet generates strong cyclonic vorticity in the boundary layer

that aids in the initiation of convection over the entire CMZ region. The convective-related monsoon rainfall variability in the CMZ is significantly correlated ( $r = 0.75$ , AD 1901–2010) to variations in the IMI (Wang et al., 2009; Goswami, 1998) region -broadly reflecting the large-scale rainfall variability in the region west of  $\sim 80^\circ\text{E}$ ) on intraseasonal (e.g. Active and Break Periods) to inter-annual (e.g. ENSO events) timescales. While the upstream processes that influence the isotopic ratio in the moisture are myriad, and therefore a direct transfer between rainfall amount and  $\delta^{18}\text{O}_p$  is not likely stationary or linear, these collective monsoonal processes are the dominant control on the annually-averaged  $\delta^{18}\text{O}_p$  variability, explaining  $\sim 25\text{--}30\%$  of the total variance of  $\delta^{18}\text{O}$  in the speleothems.

An additional monsoon reconstruction is utilized by extracting all central Indian grid points from the Monsoon Asia Drought Atlas (MADA) (Cook et al., 2010). This is a gridded network of annually-resolved JJA Palmer Drought Severity Index (PDSI) derived from over 300 tree ring width chronologies across Asia. The record extends from the present to AD 1300 and while the network contains only a single chronology from central India, the grid points from India have strong verification statistics against instrumental PDSI suggesting there is sufficient information in the network of the larger monsoon system to capture variations in the ISM. For this study, an unweighted areal average JJA PDSI between  $78$  to  $83^\circ\text{W}$  and  $14$  to  $21^\circ\text{N}$  is taken to represent a broad indicator of monsoon strength (Fig. 3). The advantage of this proxy over the speleothem record described above is that it has an absolute annually-averaged timescales and therefore no consideration of age uncertainty is needed. However, unlike the speleothem record, we presume some low frequency variability of the monsoon system reconstructed from MADA is lost during the treatment of the tree ring data (Cook et al., 1995).

### 2.1.1 ENSO Reconstructions

A number of attempts have been made to reconstruct continuous centennial to millennial length timeseries' of ENSO variability by extracting inter-annually resolved climate signals from tree rings and corals (Emile-Geay et al., 2013; Li et al., 2011; Cobb et al., 2013; Mann et al., 2009). These reconstructions are generally well-calibrated and verified though as a consequence of differences in the targeted index of ENSO to reconstruct, some significant differences can be found between the proxy records (Emile-Geay et al., 2013; Li et al., 2011). While the most accurate reconstructions of ENSO variability are presumably from proxies that are located within ENSO's center of action (i.e. the central tropical Pacific), such reconstructions are generally short and discontinuous. Proxy reconstructions from ENSO's teleconnected regions (such as the western United States) tend to be longer and continuous (e.g. Stahle et al. (1998); D'Arrigo et al. (2005)) but rely on an assumption that the

sign and strength of the teleconnection with ENSO has remained constant over time. Various ensembles of both direct and distal proxy reconstructions of ENSO show similar behavior at decadal scales but the amplitude of multidecadal to centennial variability diverges between reconstructions as a result of inherent aspects of the proxy such as hysteresis effects that favor low frequency power or the “segment length curse” (Cook et al., 1995) that favors high frequency power.

We utilize both a remote ENSO-teleconnection based tree ring proxy (Li et al., 2011) and two continuous sections (~1350-1450 and ~1630-1700) of the coral-based ENSO reconstruction of Cobb et al. (2003). The former is a millennial-length, continuous reconstruction of the canonical (eastern Pacific) ENSO amplitude derived from the first Principal Component of the gridded North American Drought Atlas (NADA) - a large dataset of tree ring based drought reconstructions (Cook et al., 2004) (Fig. 3). Li et al. (2011) derive ENSO variance by applying a biweight 21-year running variance to the first principal component of NADA. The ENSO variance generated from the tree ring network is significantly correlated to various modern indices of ENSO and arises because of the dominant influence ENSO has on moisture availability (and consequently tree growth) in water limited regions in western North America. While there is an important distinction between ENSO variance (the spread of the amplitude over a time window) versus actual interannual ENSO amplitude, variance tends to be a good proxy for El Niño strength because there is an asymmetrical quality to the ENSO system such that changes in variance tend to be driven by increases in the frequency of El Niño events (Anderson et al., 2013; Larkin and Harrison, 2002). The NADA ENSO record has excellent skill during the calibration period and agrees with shorter-term proxy reconstructions of ENSO including those derived from discontinuous coral sequences from the tropical Pacific. This record is currently the longest continuous ENSO reconstruction spanning the last millennium and has absolute annual age constraints. We utilize both the PC-1 (interannual ENSO amplitude) and the derived ENSO-variance in estimations of the relationship between ENSO and the ISM. We also utilize two multi-decadal coral  $\delta^{18}\text{O}$  sequences from Palmyra Island in the central tropical Pacific to validate our findings using an alternative to the remote-reconstruction (Fig. 3). Because of the brevity of the coral records they are not used to investigate low frequency aspects of the ENSO-ISM coupling but rather to provide an additional independent and Pacific-based proxy.

### 2.1.2 Model results

While the paper is intended to deal primarily with proxy results, analyses of the ENSO-ISM coupling is also explored

in two 1000 year control simulations using the GISS and MPI models from the CMIP5 database (Taylor et al., 2012). The analyses presented is not intended to be exhaustive but provide some insight into and a methodology to study the nature of low frequency coupling between ENSO and the ISM in state-of-the-art General Circulation Models. For both control simulations, the ISM is defined as the sum of precipitation from June-September between 78 to 83°W and 14 to 21°N and ENSO (Niño 3.4) is defined as the annually averaged SSTs for -170 to -120°W and -5 to 5°N. No additional processing was applied to the data extracted from the model simulations.

### 2.1.3 Phase Estimation

In order to assess the ENSO-ISM teleconnection, we determined the coherence and phase angle between the two systems using all combinations of the proxies listed above (e.g. coral ENSO vs. speleothem Monsoon, tree-ring ENSO vs. tree-ring Monsoon). The advantage of a spectral approach, as opposed to correlation analysis, is it allows for a delineation of the relationship between these systems at different timescales. This is critical because by combining proxies, each favoring different parts of the spectrum (tree rings and corals favoring the high frequency and speleothems favoring the low frequency), a simple correlation yields ambiguous results regarding the nature of the ENSO-ISM teleconnection. The approach follows that described by Torrence and Webster (1999) to characterize the ENSO-ISM coupling but extends the analysis into lower frequency aspects of the relationship using the longer timeseries' afforded from the proxy records. The phase angle between the overlapping periods of all the aforementioned ENSO and ISM reconstructions is done using cross-spectral analysis with the multi-taper coherence method (Chave et al., 1987). The approach is based closely on the cross-spectral analysis technique described by Huybers (2004) where coherence is assessed at progressive windows spanning the time spectrum and the phase angle is calculated by finding the lag that maximizes the correlation between the timeseries in each spectral window. For tree ring and coral proxies, the uncertainty in the phase angle is calculated using a Monte Carlo approach where the phasing of iterations of timeseries' with similar spectral properties provides confidence bounds. These timeseries' are assumed to have no age uncertainty. Uncertainty in the phase angle between the speleothem timeseries further considers the influence that age model uncertainty has in the phase angle estimation. The technique is further described in detail below.

We focus discussion hereafter on two windows of the spectra, a *high frequency* band that includes all power in the 5-15 year window and a *low frequency* band encompassing power in the 30-90 year window. The high frequency band is intended to shed light on the long-term stability of the known

dynamical connection between the ISM and ENSO during the instrumental period (Kumar et al., 1999). The high frequency band should assess variations at the interannual timescale however, as a consequence of multi-year mixing times for water in the karst, the speleothem monsoon proxy likely integrates variability across  $\sim 3$ -8 years. Therefore, we deem the 5-15 year band as the highest frequency window in which confidence in the proxy can be asserted. The low frequency window was chosen as a response to earlier work based on one of the speleothems in the composite (i.e. Berkelhammer et al. (2010)), which showed the presence of strong multidecadal power of the monsoon. The source of this multidecadal variability remains unknown as its period is too long to be studied using instrumental observations alone. The phase analysis presented here is intended, in part, to assess the role ENSO may play in pacing the dominant multidecadal power of the ISM.

To evaluate whether the differences in the phase angle between ENSO and the ISM in the low (30-90-yr.) and high (5-15-yr) frequency bands are significant against the age-model uncertainties, we performed a numerical simulation where the timescale of two sinusoidal signals (frequencies  $f_1$  and  $f_2$  with predefined phase differences of  $d_{phi}$ ) were perturbed with a gaussian random number generator. We then estimated the phase difference for the jittered series,  $d_{phi\ sim}$  using a periodogram. The standard deviation of  $d_{phi\ sim}$  for the low-frequency bound  $f_1 = 1/(30-90\ yr)$  and the high-frequency bound  $f_2 = 1/(5-15\ yr.)$  was calculated from 10,000 simulations.

The results are presented as phase wheels (Figures 4 and 6) where the direction of the arrow relative to  $0^\circ$  (due right) represents the phase angle between the timeseries'. The length of the arrows indicates the strength of the coherence and only arrows are shown where the phase angle is significant at the 90% confidence interval. The phase wheels can be interpreted as follows; a large number of arrows clustering near an angle suggests a strong likelihood that the two timeseries' exhibit coherence at that spectral window. If only a few arrows are present near an angle, there is statistically significant coherence in this band but we have less confidence that there is a persistent phase relationship in that window. All arrows that are green capture the phase angle in the high frequency window (5-15 yrs.) whereas all arrows that are purple show the phase angle in the low frequency window (30-90 yrs.). Finally, before any phase analysis was conducted, the speleothem and coral proxies were inverted such that positive values capture strong ISM periods and warm ENSO conditions, respectively. As such, the "expected" relationship between ENSO and ISM timeseries' is  $180^\circ$  (i.e. strong ENSO events being concurrent with diminished ISM precipitation).

### 3 Results

The cross spectra and phase coherence between the speleothem ISM reconstruction and NADA PC-1 amplitude timeseries' suggests that in the high frequency domain (5-15 yrs), periods of positive ENSO amplitude were associated with reduced ISM rainfall (Fig. 4a). A similar phase relationship ( $\sim 180^\circ$ ) emerges when the cross spectra between the speleothem ISM and coral ENSO reconstruction from Cobb et al. (2003) is calculated (Figure 4b). The consistency between proxies indicates that the results are robust against the choice of ENSO proxy. We find no statistically significant phase relationship between ENSO amplitude from NADA and the speleothem ISM reconstruction in the low frequency (30-90 yrs.) domain. However, if the cross-spectral analysis is done using ENSO variance from Li et al. (2011), a coherent near in-phase ( $\sim 180^\circ$ ) relationship emerges (Figure 4a). This result shows that multidecadal periods of enhanced ENSO variance were associated with generally stronger monsoons. The strength of the coherence appears to be particularly strong between AD 900 and 1500 though continues, albeit intermittently, after the 15<sup>th</sup> century (not shown). For example, some of the wettest intervals of the ISM occur after the 17<sup>th</sup> century coinciding with a multi-centennial period of the highest ENSO variance in the NADA PC-1 reconstruction. Results from the 10,000 iteration Monte Carlo simulation illustrate that even with conservative estimates of age model uncertainty, the difference in the phase angle between ENSO and the ISM timeseries' in the high and low frequency windows is significant (Figure 4). We estimate uncertainty in the phase angle estimates could be as much as  $52^\circ$  while the phase angle difference we calculate is between  $90$  to  $150^\circ$ , attesting to the robustness of this finding.

As an additional test of the ENSO-ISM coupling we also consider the phase relationship between ENSO reconstructions and the MADA-derived monsoon timeseries. In Figure 4c, the cross spectra between the two monsoon timeseries' (speleothem and tree-ring) is shown, which confirms the two systems are indeed tracking one another. While the phasing is not exactly  $0^\circ$ , as expected if the two proxies are responding to the same forcing, in the high frequency domain they generally are close to in-phase with one another. There is no statistically significant coherence between the two timeseries' in the low frequency domain, which is apparent in that the MADA timeseries misses a number of the significant sustained monsoon droughts observable in the speleothem record (Sinha et al., 2011). The MADA timeseries shows an anti-phased relationship with the NADA ENSO amplitude, further confirming the robustness of the finding that positive ENSO amplitude is associated with a weakened ISM (Figure 4d). There is some indication of a  $90^\circ$  phase angle in the low frequency window, but the coherence is of low significance. Finally,

we test the coherence between ENSO and the ISM using the coral ENSO and MADA ISM proxies (Figure 4e). The results here provide further evidence of coherent coupling between ENSO and the ISM in the high frequency that is insensitive to ENSO or ISM proxy choice. Because a number of the proxies are unsuited for exploring the low frequency phasing, we were not able to confirm the unique phase angle observed between NADA ENSO variance and the speleothem ISM. Given the strong independent skill each of these two proxies have in capturing their targeted field and that the coherence between them in the low frequency domain is high, we have confidence that the unique low frequency coherence and phase angle is robust.

To compare the proxy observations with the model simulations, we calculate the coherence and phase angle between the model-derived ENSO and ISM timeseries' (Figure 5). The cross spectral analysis using results from the GISS model, show that in the high frequency domain, positive (negative) ENSO amplitude leads to a weakened (strengthened) ISM with a very high degree of confidence (Figure 6a). In the low frequency domain, we also find some indication of a reversal of this phasing, similar to that was observed with the proxies (Figure 4). However, we acknowledge that the statistical significance of the phasing in the low frequency is weak (judging by the small number of arrows). The MPI model also shows the same relationship as with the GISS model in the high frequency domain (inverse relationship) (Figure 6b). However, contrary to GISS, the MPI simulation suggests a similar phase relationship between ENSO and the ISM in both the high and low frequency domains.

#### 4 Discussion

An important finding that emerges from the study is that irrespective of proxy choice, there is a persistent high frequency coupling between the ISM and ENSO. The dynamics of this coupling (weak monsoon during positive ENSO) has been discussed extensively with respect to instrumental data (e.g. (Kumar et al., 2006)). The proxy data thus suggests there is a consistent influence of ENSO on the ISM over the last millennium. The nature of this coupling is also captured in the two model simulation analyzed here. An important question that we can now assess with the proxy data is whether the persistent high-frequency ENSO-ISM coupling can explain the presence of strong multidecadal power in the ISM. Our *a priori* expectation was that because enhanced ENSO variance is driven by more frequent El Niño's, multidecadal periods of increased (decreased) ENSO variance would drive sustained periods of weakened (strengthened) ISM rainfall. Therefore, changes in the frequency of large or persistent El Niño's would produce low frequency variability in ISM rainfall. The results presented in Figure 4a imply,

counterintuitive to our expectation, that a more active ENSO state occurs simultaneously with an increase in ISM rainfall. While we acknowledge the challenges and uncertainty in deriving low frequency ENSO variance from NADA, a few pointed examples of periods of enhanced ENSO variance associated with a weakened ISM provide confidence in this finding. For example, the major ISM droughts of the late 14<sup>th</sup> century occur in the context of reduced ENSO variance based independently on the coral-based ENSO proxy of Cobb et al. (2003).

A number of mechanisms could explain the fact that periods of enhanced ENSO variance occur simultaneously with a strengthened ISM. One possible explanation is that changes in ENSO variance are actually driven by an increase in La Niña events. This is somewhat contradictory to the assumed driver of changes in ENSO variance (Anderson et al., 2013), but if this was the case, periods of high variance would be associated with more La Niña events and consequently a stronger ISM. However, an analysis of the reconstructed ENSO distribution during periods of high variance, do not indicate an asymmetry that favors La Niña (Fig. 7). The distribution, in fact, slight favors El Niño during periods of high variance, consistent with observational records and modeling studies (Timmermann et al., 2005; Larkin and Harrison, 2002). An alternative explanation is that in the low frequency domain the two systems are phase-locked through a common forcing mechanism, which leads to both an increase (decrease) in ENSO variance and a strengthened (weakened) ISM. Candidates for this forcing mechanism must also contain strong multidecadal power.

One mechanism to explain the presence of shared multidecadal power between these systems is through periodic variability in the North Atlantic SSTs. It is well-documented that North Atlantic SSTs are characterized by power with 50-90 year periodicity (Enfield et al., 2001) and have an impact on both ENSO variance and ISM rainfall. Goswami et al. (2006) show that much of the multidecadal power of ISM rainfall during the instrumental period can be linked to shifts in North Atlantic SSTs. The authors argue that warming in the North Atlantic influences tropospheric temperatures over Eurasia and consequently the meridional temperature gradient over India. This change in the temperature gradient, in turn, leads to an increase in ISM rainfall. A similar finding has been shown on millennial timescales where warmer conditions in the North Atlantic are associated with a stronger monsoon (Gupta et al., 2003). A number of studies have also looked at the impact that changes in the North Atlantic SST fields have on ENSO variance. Timmermann et al. (2005) show that cooling of the North Atlantic leads to a deepening of the tropical Pacific thermocline, which stabilizes the ENSO system (i.e. reduces variance). While their analysis focused on millennial-scale events, the oceanic teleconnection mechanism they de-

scribe also appears to operate on multidecadal timescales. 635  
Therefore, positive (negative) SSTs in the North Atlantic  
would lead to both an increase (decrease) in ISM rainfall  
and ENSO variance. However, it must also be noted that  
the link between ENSO variance and North Atlantic SSTs  
proposed by (Timmermann et al., 2005) is contrary to the 640  
findings of Dong et al. (2006) who describe the presence of  
an atmospheric bridge where cooling in the North Atlantic,  
reduces easterly flow in the tropical Pacific leading to a  
shallower thermocline and *enhanced* ENSO variance. The  
difference between the findings of these studies is likely 645  
embedded in the fact that the former (i.e. Timmermann et al.  
(2005)) focussed on an oceanic teleconnection while the  
latter (i.e. Dong et al. (2006)) focussed on an atmospheric  
bridge. Because we are interested here primarily in the  
low frequency nature of the ENSO-ISM coupling, it is 650  
appropriate to consider the oceanic mechanism as it would  
have a characteristic tendency for lower frequency power.

Lastly, a number of recent studies such as Tierney et al.  
(2013) argue for a dominant role of dynamics internal to the 655  
Indian Ocean (IO) in producing multidecadal hydroclimate  
variability across the IO Basin. IO dynamics are indeed a  
critical source of variance in the monsoon (Ashok et al.,  
2004) and likely an important determinant of low frequency  
monsoon behavior (Sinha et al., 2011). If the multidecadal 660  
power in the ISM is paced by internal dynamics in the  
IO, than the phasing between ENSO and the ISM shown  
here brings about a number of questions regarding the  
relationship between IO dynamics and the ENSO system.  
For example, if basin-wide shifts in the IO are influencing 665  
shifts in ENSO variance than the results here suggest that  
the IO's direct influence on the monsoon is stronger than  
from the teleconnections that influence the ISM through  
ENSO. Additional analyses, including high-resolution  
proxy reconstructions of IO SSTs (and east-west IO SST 670  
gradients) as well as modeling simulations would be needed  
to constrain whether IO, North Atlantic or additional dynamical  
mechanisms are driving the coupling between ENSO  
variance and ISM rainfall in the low frequency domain. A  
first step towards resolving this might be in isolating model  
simulations that reproduce the observed phase difference 675  
between ENSO-ISM coupling in the high and low frequency  
domains. There is some indication in Figure 6 that realistic  
phasing between the systems may emerge in some models 675  
but a larger ensemble of models would ultimately be needed  
to isolate the likely mechanism that couples these systems.

## 5 Conclusions

Over the last millennium, the ISM has exhibited persistent  
multidecadal power. The protracted multidecadal shifts  
in precipitation amounts are significant in considering both

flooding and drought frequency in India. The susceptibility  
of agricultural production to these hydroclimatic changes  
may increase in coming decades as regional groundwater  
resources have been severely depleted and therefore may not  
be able to provide a buffer (Rodell et al., 2009). Through  
analyses of the phase relationship between proxies for ENSO  
and the ISM, we show that high frequency (5-15 yrs) shifts  
in ENSO amplitude yielded a persistent influence on ISM  
rainfall likely through a previously documented atmospheric  
teleconnection (Kumar et al., 2006). However, in the low  
frequency domain (30-90 yrs), periods of increased ENSO  
variance were coincident with an increase in ISM rainfall.  
This suggests that the dynamic that couples the systems in  
the high frequency domain is not the same as that which  
couples them in the low frequency domain. One plausible  
mechanism to explain this observation is that low frequency  
changes in North Atlantic SSTs lead to multidecadal  
phase-locking between ISM rainfall and ENSO variance.  
This arises due to the presence of an atmospheric  
teleconnection between the North Atlantic and the ISM  
and an oceanic teleconnection between the North Atlantic  
and ENSO variance. Another plausible mechanism involves  
low frequency behavior within the Indian Ocean, that has  
a known influence on the ISM rainfall and may also have  
a causal link with ENSO. Additional proxy data from the  
Indian Ocean are needed to resolve the prominence of this  
dynamic. The ENSO system has experienced increased  
variance during the late 20<sup>th</sup> century. If the trend in  
ENSO variance continues, the results presented here do  
not suggest this will lead to a weakened monsoon. In  
fact, if the coupling between the systems during the  
proxy-era remains stable, the opposite trend (an increase  
in ISM rainfall) would be more likely. An assessment of  
model simulated ENSO and ISM rainfall under different  
radiative forcing scenarios would be needed to lend  
confidence to this and one method to isolate model  
simulations that correctly capture the coupling between  
the systems is presented here.

*Acknowledgements.* We gratefully acknowledge the National  
Science Foundation grant to A.S. (ATM: 0823554) and Chinese  
National Science Foundation support to H.C. for funding a  
portion of this research.

## References

### References

- Anderson, B. T., Furtado, J. C., Cobb, K. M., and Di Lorenzo, E.:  
Extratropical forcing of El Niño–Southern Oscillation asymmetry,  
Geophysical Research Letters, 2013.
- Annamalai, H., Hamilton, K., and Sperber, K.: The South Asian  
summer monsoon and its relationship with ENSO in the IPCC  
AR4 simulations, *Journal of Climate*, 20, 1071–1092, 2007.
- Ashok, K., Guan, Z., Saji, N., and Yamagata, T.: Individual and  
combined influences of ENSO and the Indian Ocean dipole on

- the Indian summer monsoon, *Journal of Climate*, 17, 3141–3155, 2004. <sup>745</sup>
- Berkelhammer, M., Sinha, A., Mudelsee, M., Cheng, H., Edwards, R. L., and Cannariato, K.: Persistent multidecadal power of the Indian Summer Monsoon, *Earth and Planetary Science Letters*, 290, 166–172, 2010. <sup>690</sup>
- Berkelhammer, M., Sinha, A., Stott, L., Cheng, H., Pausata, F., and Yoshimura, K.: An abrupt shift in the Indian monsoon 4000 years ago, *Geophysical Monograph Series*, 198, 75–87, 2012. <sup>750</sup>
- Buckley, B. M., Anchukaitis, K. J., Penny, D., Fletcher, R., Cook, E. R., Sano, M., Nam, L. C., Wichienkeo, A., Minh, T. T., and Hong, T. M.: Climate as a contributing factor in the demise of Angkor, Cambodia, *Proceedings of the National Academy of Sciences of the United States of America*, 107, 6748, 2010. <sup>695</sup>
- Chave, A. D., Thomson, D. J., and Ander, M. E.: On the robust estimation of power spectra, coherences, and transfer functions, *Journal of Geophysical Research*, 92, 633–648, doi:<http://dx.doi.org/10.1029/JB092iB01p0063310>.1029/JB092iB01p0063310, 1987. <sup>700</sup>
- Cobb, K. M., Charles, C. D., Cheng, H., and Edwards, R. L.: El Niño/Southern Oscillation and tropical Pacific climate during the last millennium, *Nature*, 424, 271–276, 2003. <sup>705</sup>
- Cobb, K. M., Westphal, N., Sayani, H. R., Watson, J. T., Di Lorenzo, E., Cheng, H., Edwards, R., and Charles, C. D.: Highly Variable El Niño–Southern Oscillation Throughout the Holocene, *Science*, 339, 67–70, 2013. <sup>710</sup>
- Collins, M., An, S.-I., Cai, W., Ganachaud, A., Guilyardi, E., Jin, F.-F., Jochum, M., Lengaigne, M., Power, S., Timmermann, A., Vecchi, G., and Wittenberg, A.: The impact of global warming on the tropical Pacific Ocean and El Niño, *Nature Geoscience*, 3, 391–397, 2010. <sup>715</sup>
- Cook, E. R., Briffa, K. R., Meko, D. M., Graybill, D. A., and Funkhouser, G.: The ‘segment length curse’ in long tree-ring chronology development for palaeoclimatic studies, *The Holocene*, 5, 229–237, 1995. <sup>720</sup>
- Cook, E. R., Woodhouse, C. A., Eakin, C. M., Meko, D. M., and Stahle, D. W.: Long-term aridity changes in the western United States, *Science*, 306, 1015–1018, 2004. <sup>725</sup>
- Cook, E. R., Anchukaitis, K. J., Buckley, B. M., Drrigo, R. D., Jacoby, G. C., and Wright, W. E.: Asian monsoon failure and megadrought during the last millennium, *Science*, 328, 486–489, 2010. <sup>730</sup>
- Dansgaard, W.: Stable isotopes in precipitation, *Tellus*, 16, 436–468, 1964. <sup>735</sup>
- D’Arrigo, R., Cook, E. R., Wilson, R. J., Allan, R., and Mann, M. E.: On the variability of ENSO over the past six centuries, *Geophysical Research Letters*, 32, L03 711, 2005.
- Dayem, K. E., Molnar, P., Battisti, D. S., and Roe, G. H.: Lessons learned from oxygen isotopes in modern precipitation applied to interpretation of speleothem records of paleoclimate from eastern Asia, *Earth and Planetary Science Letters*, 295, 219–230, 2010. <sup>740</sup>
- Dong, B., Sutton, R. T., and Scaife, A. A.: Multi-decadal modulation of El Niño–Southern Oscillation (ENSO) variance by Atlantic Ocean sea surface temperatures, *Geophysical Research Letters*, 33, L08 705, doi:<http://dx.doi.org/10.1029/2006GL025766>.1029/2006GL025766, 2006. <sup>800</sup>
- Draxler, R. and Rolph, G.: HYSPLIT (HYbrid Single-Particle Lagrangian Integrated Trajectory) model access via NOAA ARL READY website (<http://www.arl.noaa.gov/ready/hysplit4.html>). NOAA Air Resources Laboratory, Silver Spring, 2003.
- Emile-Geay, J., Cobb, K. M., Mann, M. E., and Wittenberg, A. T.: Estimating Central Equatorial Pacific SST variability over the Past Millennium. Part 2: Reconstructions and Implications, *Journal of Climate*, 2013.
- Enfield, D. B., Mestas-Nuñez, A. M., and Trimble, P. J.: The Atlantic Multidecadal Oscillation and its relation to rainfall and river flows in the continental US, *Geophysical Research Letters*, 28, 2077–2080, 2001.
- Fasullo, J. and Webster, P.: Hydrological signatures relating the Asian summer monsoon and ENSO, *Journal of climate*, 15, 3082–3095, 2002.
- Gershunov, A., Schneider, N., and Barnett, T.: Low-frequency modulation of the ENSO-Indian monsoon rainfall relationship: Signal or noise?, *Journal of Climate*, 14, 2486–2492, 2001.
- Goswami, B.: Interannual variations of Indian summer monsoon in a GCM: External conditions versus internal feedbacks, *Journal of climate*, 11, 501–522, 1998.
- Goswami, B. N., Madhusoodanan, M., Neema, C., and Sengupta, D.: A physical mechanism for North Atlantic SST influence on the Indian summer monsoon, *Geophysical Research Letters*, 33, L02 706\_1–L02 706\_4, doi:<http://dx.doi.org/10.1029/2005GL024803>.1029/2005GL024803, 2006.
- Gupta, A. K., Anderson, D. M., and Overpeck, J. T.: Abrupt changes in the Asian southwest monsoon during the Holocene and their links to the North Atlantic Ocean, *Nature*, 421, 354–357, 2003.
- Huybers, P.: Comment on ‘Coupling of the hemispheres in observations and simulations of glacial climate change’ by A. Schmittner, O. Saenko, and A. Weaver, *Quaternary Science Reviews*, 23, 207–210, doi:<http://dx.doi.org/10.1016/j.quascirev.2003.08.001>.1016/j.quascirev.2004. <sup>2004.</sup>
- Jourdain, N. C., Gupta, A. S., Taschetto, A. S., Ummenhofer, C. C., Moise, A. F., and Ashok, K.: The Indo-Australian monsoon and its relationship to ENSO and IOD in reanalysis data and the CMIP3/CMIP5 simulations, *Climate Dynamics*, pp. 1–30, 2013.
- Krishnamurthy, V. and Goswami, B. N.: Indian monsoon-ENSO relationship on interdecadal timescale, *Journal of Climate*, 13, 579–595, 2000.
- Kumar, K. K., Rajagopalan, B., and Cane, M. A.: On the weakening relationship between the Indian monsoon and ENSO, *Science*, 284, 2156–2159, 1999.
- Kumar, K. K., Rajagopalan, B., Hoerling, M., Bates, G., and Cane, M.: Unraveling the mystery of Indian monsoon failure during El Niño, *Science*, 314, 115–119, 2006.
- Larkin, N. K. and Harrison, D.: ENSO warm (El Niño) and cold (La Niña) event life cycles: Ocean surface anomaly patterns, their symmetries, asymmetries, and implications, *Journal of Climate*, 15, 1118–1140, 2002.
- Li, J., Xie, S.-P., Cook, E. R., Huang, G., D’Arrigo, R., Liu, F., Ma, J., and Zheng, X.-T.: Interdecadal modulation of El



- Niño amplitude during the past millennium, *Nature Climate Change*, 1, 114–118, 2011.
- 805 Mann, M. E., Zhang, Z., Rutherford, S., Bradley, R. S., Hughes, M. K., Shindell, D., Ammann, C., Faluvegi, G., and Ni, F.: 865 Global signatures and dynamical origins of the Little Ice Age and Medieval Climate Anomaly, *Science*, 326, 1256–1260, 2009.
- 810 Mudelsee, M.: *Climate time series analysis: classical statistical and bootstrap methods*, vol. 42, Springer, 2010. 870
- Pausata, F. S., Battisti, D. S., Nisancioglu, K. H., and Bitz, C. M.: Chinese stalagmite [ $\delta^{18}O$ ] controlled by changes in the Indian monsoon during a simulated Heinrich event, *Nature Geoscience*, 4, 474–480, 2011.
- 815 Rodell, M., Velicogna, I., and Famiglietti, J. S.: Satellite-based 875 estimates of groundwater depletion in India, *Nature*, 460, 999–1002, 2009.
- 820 Sinha, A., Cannariato, K. G., Stott, L. D., Cheng, H., Edwards, R. L., Yadava, M. G., Ramesh, R., and Singh, I. B.: A 900-year (600 to 1500 AD) record of the Indian summer monsoon precipitation from the core monsoon zone of India, *Geophysical Research Letters*, 34, L16 707, doi:<http://dx.doi.org/10.1029/2007GL030431>.1029/2007GL030431, 2007.
- 825 Sinha, A., Berkelhammer, M., Stott, L., Mudelsee, M., Cheng, H., and Biswas, J.: The leading mode of Indian Summer Monsoon precipitation variability during the last millennium, *Geophysical Research Letters*, 38, L15 703, doi:<http://dx.doi.org/10.1029/2011GL047713>.1029/2011GL047713, 2011.
- 830 Stahle, D. W., Cleaveland, M., Therrell, M., Gay, D., D'arrigo, R., Krusic, P., Cook, E., Allan, R., Cole, J., Dunbar, R., et al.: Experimental dendroclimatic reconstruction of the Southern Oscillation, *Bulletin of the American Meteorological Society*, 79, 2137–2152, 1998.
- 835 Taylor, K. E., Stouffer, R. J., and Meehl, G. A.: An overview of CMIP5 and the experiment design, *Bulletin of the American Meteorological Society*, 93, 485–498, 2012.
- 840 Tierney, J. E., Smerdon, J. E., Anchukaitis, K. J., and Seager, R.: Multidecadal variability in East African hydroclimate controlled by the Indian Ocean, *Nature*, 493, 389–392, 2013.
- Timmermann, A., An, S., Krebs, U., and Goosse, H.: ENSO Suppression due to Weakening of the North Atlantic Thermohaline Circulation\*, *Journal of Climate*, 18, 3122–3139, 2005.
- 845 Torrence, C. and Webster, P. J.: Interdecadal changes in the ENSO-monsoon system, *Journal of Climate*, 12, 2679–2690, 1999.
- 850 Ummenhofer, C. C., Gupta, A. S., Li, Y., Taschetto, A. S., and England, M. H.: Multi-decadal modulation of the El Niño–Indian monsoon relationship by Indian Ocean variability, *Environmental Research Letters*, 6, 034 006, doi:<http://dx.doi.org/10.1088/1748-9326/6/3/034006>.1088/1748-9326/6/3/034006, 2011.
- 855 Vuille, M., Werner, M., Bradley, R., and Keimig, F.: Stable isotopes in precipitation in the Asian monsoon region, *Journal of geophysical research*, 110, D23 108–1, doi:<http://dx.doi.org/10.1029/2005JD006022>.1029/2005JD006022, 2005.
- 860 Wang, B. and Fan, Z.: Choice of South Asian summer monsoon indices, *BULLETIN-AMERICAN METEOROLOGICAL SOCIETY*, 80, 629–638, 1999.
- Wang, B., Ding, Q., and Joseph, P.: Objective Definition of the Indian Summer Monsoon Onset, *Journal of Climate*, 22, 3303–3316, 2009.
- Webster, P. J., Magaña, V., Palmer, T., Shukla, J., Tomas, R., Yanai, M., and Yasunari, T.: Monsoons: Processes, predictability, and the prospects for prediction, *Journal of Geophysical Research*, 103, 14 451–14 510, doi:<http://dx.doi.org/10.1029/97JC02719>.1029/97JC02719, 1998.
- Yoshimura, K., Kanamitsu, M., Noone, D., and Oki, T.: Historical isotope simulation using reanalysis atmospheric data, *Journal of Geophysical Research*, 113, D19 108, doi:<http://dx.doi.org/10.1029/2008JD010074>.1029/2008JD010074, 2008.
- ...

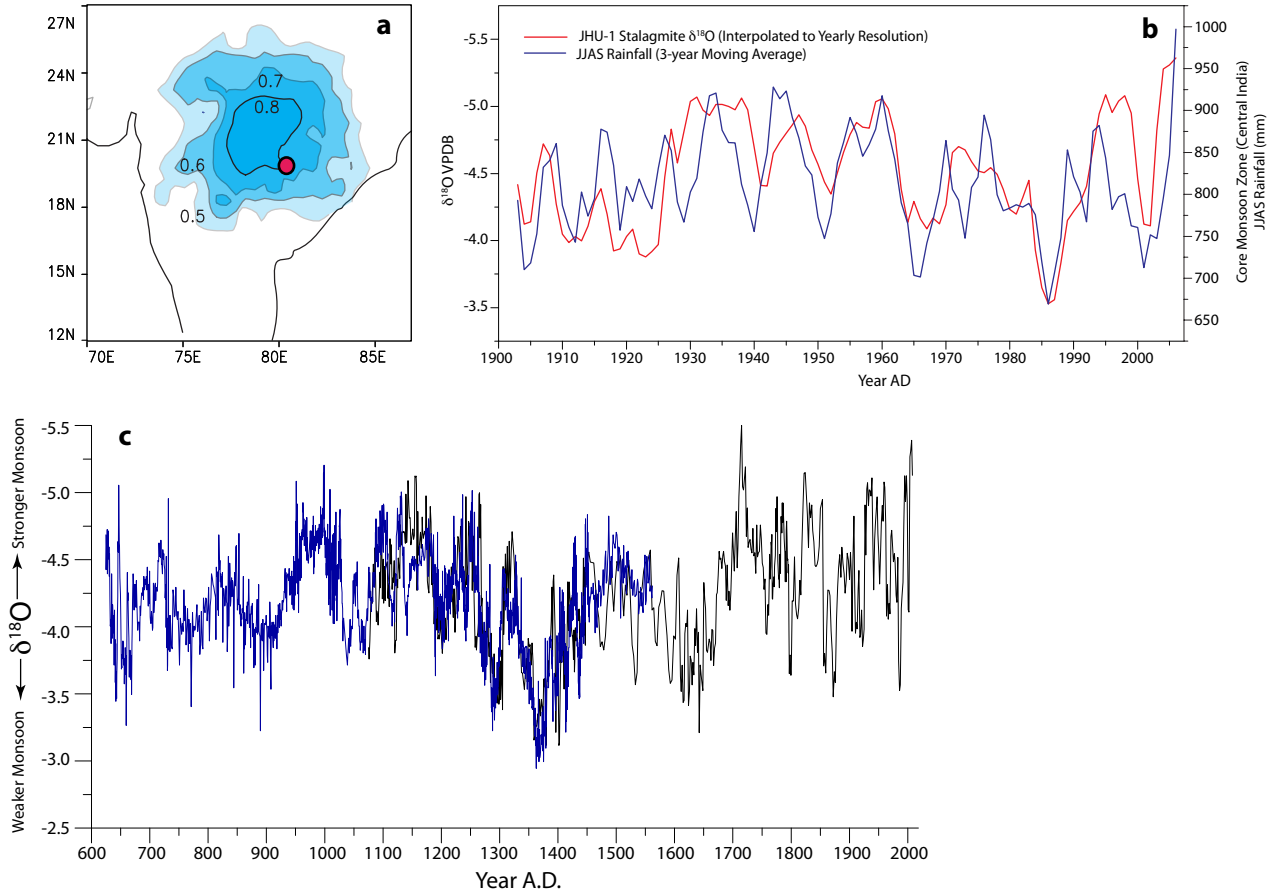


**Fig. 1.** (a) Correlation map between JJAS precipitation and regional precipitation across India. The result indicates the significance of this site as a broad indicator of CMZ monsoon precipitation. (b) The 20<sup>th</sup> century section of the speleothem  $\delta^{18}\text{O}$  and JJAS rainfall. The observed precipitation amounts were treated with a 3-year smooth to mimic mixing of waters in the karst. (c) The complete  $\delta^{18}\text{O}$  timeseries from the JHU-1 (black) and Dandak (blue) records. Details of these records can be found in Sinha et al. (2011) and Berkelhammer et al. (2010).

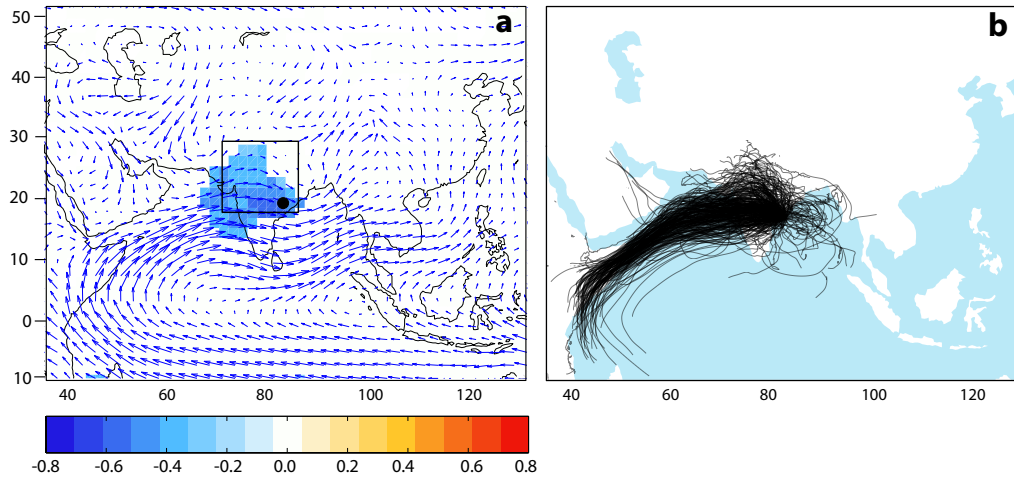


**Fig. 2.** (a) Correlation between JJAS  $\delta^{18}O_p$  from nearest grid cell to the proxy and the precipitation rates in the surrounding grid cells using the IsoGSM model of Yoshimura et al. (2008). The analysis shows how upstream precipitation across India become aggregated in  $\delta^{18}O_p$  at the proxy site. The vectors indicate the average surface wind fields during JJAS. (b) A composite of 2400 trajectories from 2002-2011 using the Hysplit model (Draxler and Rolph, 2003). Each trajectory was run for 90 hours from the proxy site and initialized twice per day at UTC 06 and UTC 12 at 1500 meters above ground level.

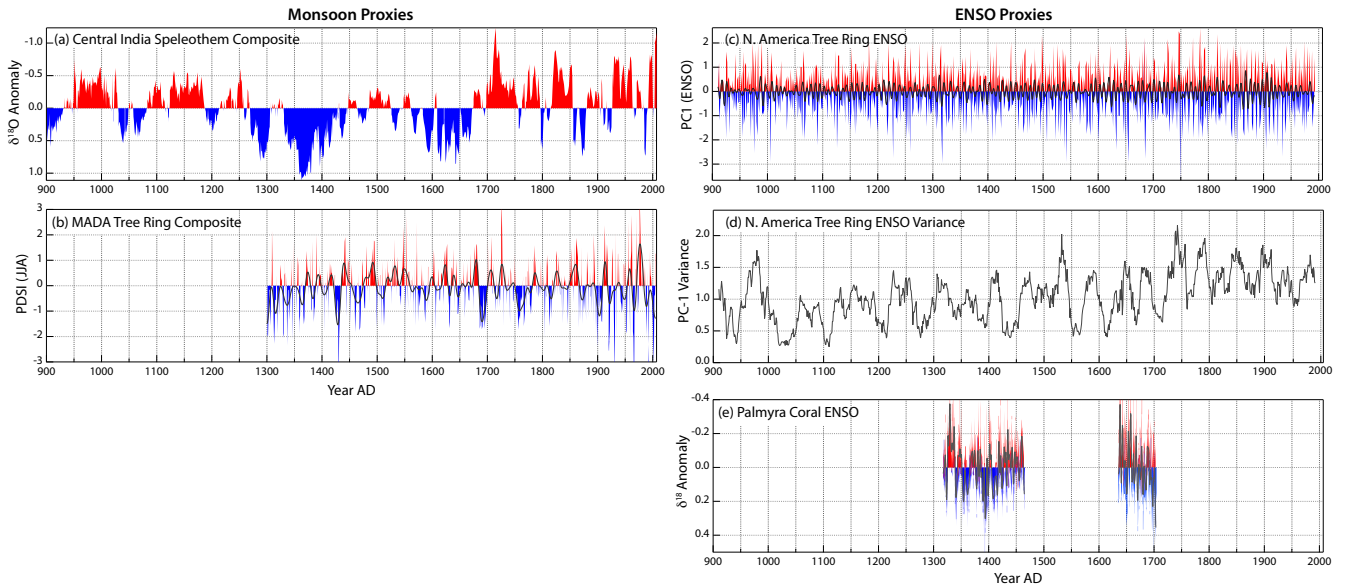


**Fig. 3.** (a) Annually interpolated speleothem monsoon reconstruction from Figure 1 shown as isotopic ( $\delta^{18}O$ ) anomalies relative to the mean of the timeseries. Y-axis is reversed so that dry periods point down. (b) The central Indian monsoon reconstruction based on the average of all grid points in central India from the MADA database (Cook et al., 2010). A lanczos filter is applied to the data to accentuate variability in the 5-15 year window. (c) The first principal component of the NADA network from Li et al. (2011), which largely reflects SSTs in the eastern Tropical Pacific. A similar bandpass filter is applied to the data as in Panel B. (d) The bi-weight variance of the PC-1 of the NADA ENSO reconstruction (Li et al., 2011). (e) Two long continuous sections of the Palmyra coral  $\delta^{18}O$  timeseries' from Cobb et al. (2003). As in Panel A, the y-axis is reversed so that warm SSTs are up.

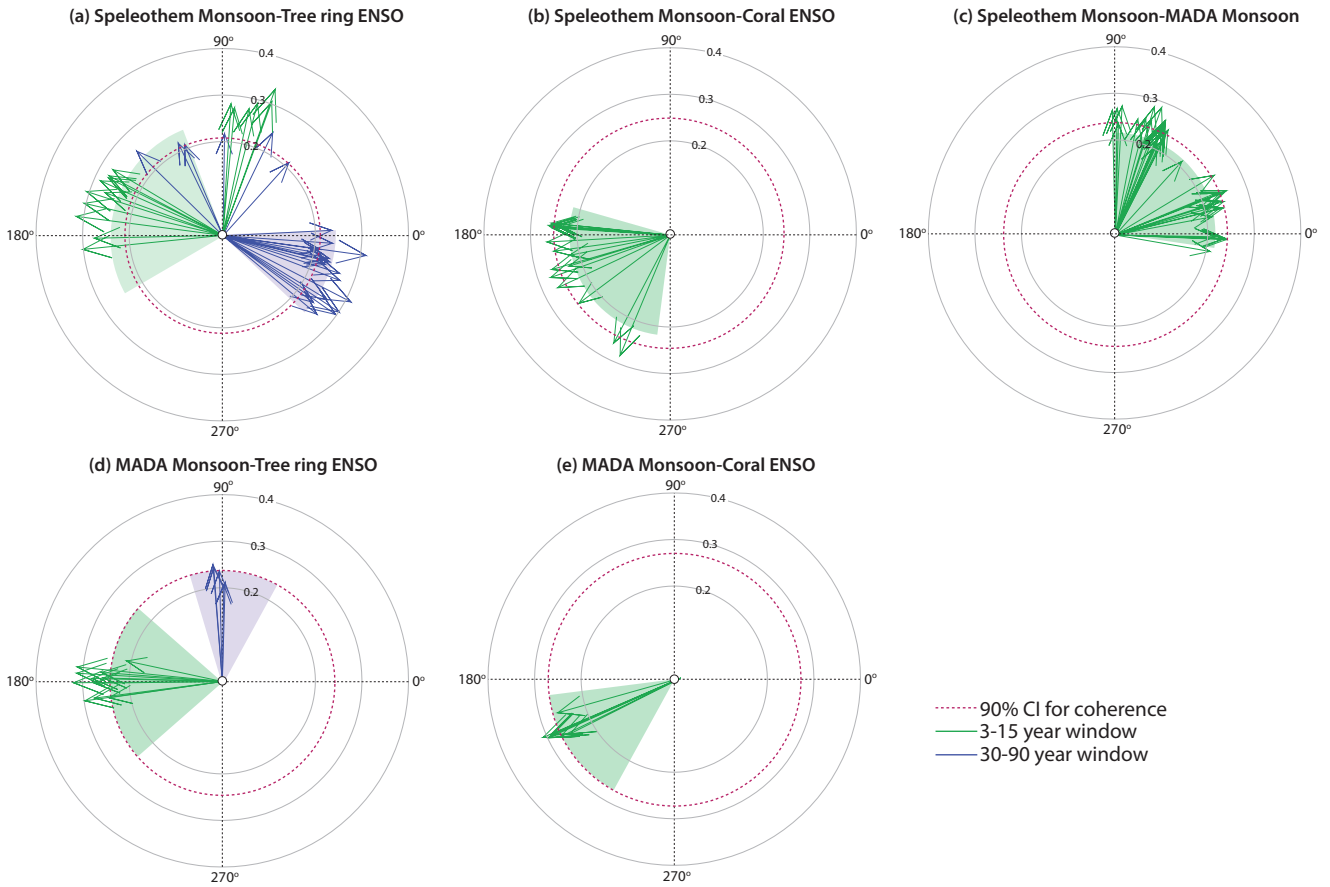


**Fig. 4.** Results from cross spectral analysis between all proxy timeseries shown in Figure 3. Arrows to the right indicate timeseries that are in phase with one another while arrows to the left indicate timeseries that are anti-phased. Only arrows are shown when coherence between the timeseries' is significant at the 90% confidence interval. The length of the arrow indicates the strength of the coherence and the concentric circles indicate increasing (labeled) levels of coherence. The shaded wedges indicate estimates of uncertainty which accounts both for age model uncertainties and that which arises from noise in the timeseries'. All green arrows and wedges are for phasing in the high frequency (5-15 yrs) window and purple arrows and wedges are for phasing in the low frequency (30-90 yrs.) windows. Lastly, the speleothem and coral timeseries' were inverted such that for all analyses arrows to the left (right) indicate strong (weak) monsoon associated with weak ENSO. (a) Speleothem ISM (Sinha et al., 2011) against tree ring ENSO (Li et al., 2011), (b) Speleothem ISM (Sinha et al., 2011) against coral ENSO (Cobb et al., 2003), (c) Speleothem ISM (Sinha et al., 2011) against MADA ISM (Cook et al., 2010), (d) MADA ISM (Cook et al., 2010) against tree ring ENSO (Li et al., 2011) and (e) MADA ISM (Cook et al., 2010) against coral ENSO (Cobb et al., 2003)

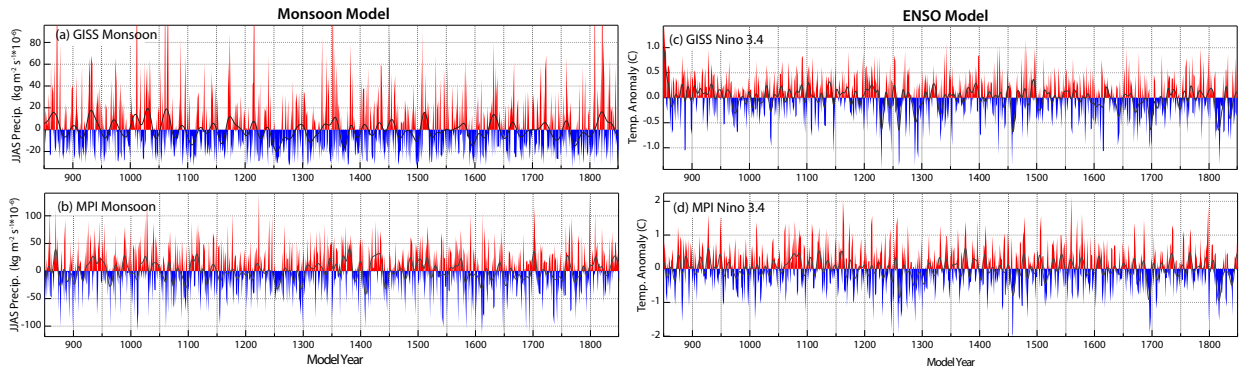


**Fig. 5.** Timeseries of the monsoon (left) and Nino3.4 (right) from the GISS (top) and MPI (bottom) models. The ISM precipitation is the sum of JJAS precipitation over India and the ENSO timeseries is the annually-averaged SSTs over the Niño 3.4 region. These 1000-year monthly-resolved data were taken from the CMIP5 database (Taylor et al., 2012). No additional processing such as normalization were applied to the data.

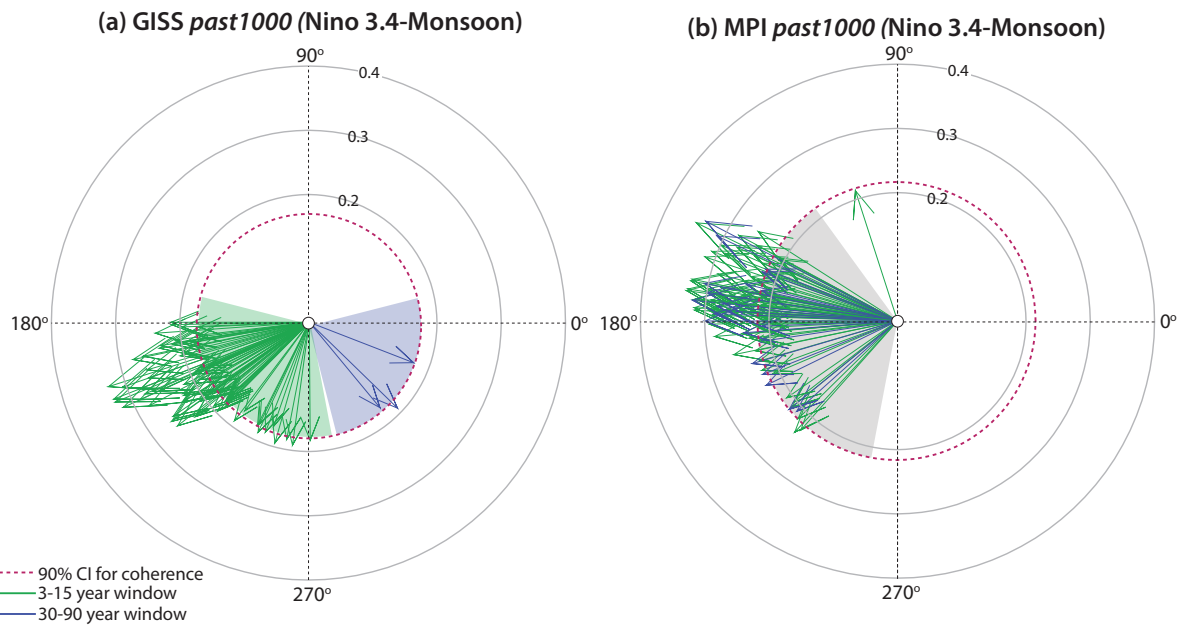


**Fig. 6.** Phase relationships between ENSO and the ISM for the two modeled timeseries in Figure 5. Phase wheels can be interpreted identically to those shown in Figure 4.

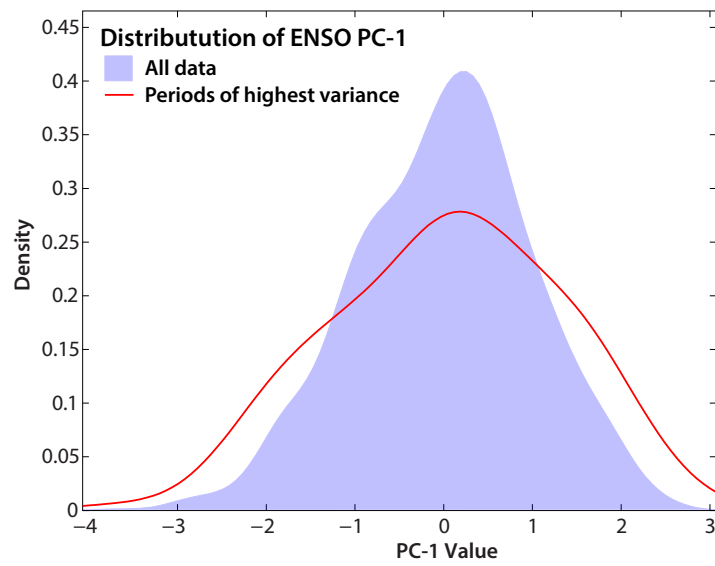


**Fig. 7.** Distribution of the annual PC-1 scores from Li et al. (2011) using all data (blue shading) and during windows of increased variance ( $\geq 1.5$ , Panel D Figure 3). The distribution is wider during periods of increased variance but does not have a tail favoring La Niña. The data suggests a preference for El Niño during enhanced variance but not with strong statistical confidence.